Research Article SOHAG JOURNAL OF SCIENCES

DOI: 10.21608/sjsci.2025.395525.1286

New Perspectives on Quantum Teleportation and Entropic Uncertainty in a Nonlinear Two-Atom System

Haytham Bakry[*,1], *Nour Zidan*[1,2], *Ali H. Homid*[3] *and Mahmoud Abdel-Aty*[1,4,5]

[1] Faculty of Science, Sohag University, Sohag 82524, Egypt.
[2] Mathematics Department, College of Science, Jouf University, Sakaka 72341, Saudi Arabia.
[3] Faculty of Science, Al-Azhar University, Assiut 71524, Egypt.
[4]Electrical and Computer Engineering Department, Abu Dhabi University, United Arab Emirates
[5]Deanship of Graduate Studies and Research, Ahlia University, P.O. Box 10878 Manama, Bahrain
[*]**Corresponding Author:** haitham.bakry@science.sohag.edu.eg.

Received: 1st July 2025., Revised: 30th July 2025., Accepted: 7th August 2025.
Published online: 17th August 2025.

Abstract:

In this paper, we examine two crucial aspects of quantum information processing: the dynamics of entanglement in atom-field interactions and the fidelity of quantum teleportation under nonlinear effects. We analyze entanglement and quantum entropic uncertainty in a system of two-level atoms coupled to a Fock-state cavity field, taking into account the effects of the Kerr medium and the Stark shift. Our findings reveal phenomena such as entanglement, sudden death, and revival, with these occurrences becoming more frequent at higher Kerr and Stark parameters. Furthermore, we investigate the dynamics of average fidelity in a quantum teleportation protocol, focusing on the roles of the input state angle θ and the nonlinear coupling strength χ_1. Fideism exhibits periodic behavior, achieving optimal values in specific parameter settings, particularly when $\theta = \pi$. These insights significantly enhance our understanding of quantum entanglement control and high-fidelity teleportation, which are essential for advancing quantum communication, cryptography, and measurement protocols.

Keywords: Witness of entanglement, Entropic Uncertainty, Kerr medium, Fidelity, Teleportation.

1 Introduction

The uncertainty principle lies at the heart of quantum mechanics, providing a foundational distinction between classical and quantum behavior. It can be formulated in two primary ways. The first is Heisenberg's uncertainty principle, which quantifies the product of the standard deviations of two noncommuting observables M and N as $\Delta M \cdot \Delta N \geq \frac{1}{2}|\langle [M,N] \rangle|$ [1]. This relation emphasizes the fundamental limit to the precision with which two incompatible observables can be known simultaneously.

The second formulation is the entropic uncertainty relation, which utilizes Shannon entropy to express uncertainty in measurement outcomes [2,3,4]. For a result of measurement z from a probability distribution $p(z)$, the Shannon entropy is defined as $S(Z) = -\sum_l p_l(z) \log_2 p_l(z)$. For two incompatible observables M and N, the entropic uncertainty relation takes the form $S(M) + S(N) \geq \log_2 \left(\frac{1}{c}\right)$, where $1/c$ represents the complementarity of the observables and is given by $c \equiv \max_{r,s} |\langle \varphi_r | \psi_s \rangle|^2$, with $|\varphi_r\rangle$ and $|\psi_s\rangle$ being the eigenvectors of M and N, respectively.

A more general formulation of this principle, incorporating quantum memory, has been proposed in [5] as:

$$S(M|B) + S(N|B) \geq \log_2 \left(\frac{1}{c}\right) + S(A|B), \qquad (1)$$

where $S(A|B) = S(\rho_{AB}) - S(\rho_B)$ is the conditional von Neumann entropy. The quantum memory-assisted entropic uncertainty relation has attracted significant attention for its role in understanding quantum correlations and information processing in open quantum systems [6,7]. Quantum memory-assisted entropic uncertainty, Jensen-Shannon coherence, and entanglement dynamics in a graphene sheet with disordered electrons affected by intrinsic decoherence were studied [8]. Entropy uncertainty relations

considering quantum memory and entanglement for non-orthogonal states built from two-qubit coherent states were analyzed [9]. The entropic uncertainty relations and quantum coherence in the two-dimensional XXZ spin model with Dzyaloshinskii–Moriya interaction were investigated [10]. The relation between the quantum memory-assisted entropic uncertainty relation and the quantum phase transition in the spin XXZ model was examined. The results indicate that the entropic uncertainty and its lower bound exhibit similar characteristics [11]. One of the most intriguing quantum phenomena underpinning modern quantum technologies is entanglement [12,13,14,15]. It plays a central role in quantum teleportation, quantum dense coding, quantum key distribution, and quantum computing [16,17,18,19,20,21,22]. However, entanglement is often fragile in realistic settings as a result of decoherence and dissipation from the environment. Consequently, preserving entanglement in open systems has become a critical area of research [23,24]. The entropic uncertainty principle has also been shown to be effective in detecting entanglement in various system-reservoir configurations [25].

In recent studies, the lower bound of the entropic uncertainty relation has been applied to examine the dynamics of entanglement in atomic systems coupled to non-Markovian reservoirs [26]. Further investigations have demonstrated connections between entropic uncertainty, quantum memory, and entanglement witness criteria. Numerous works have also explored the role of external influences such as Stark shifts, Kerr nonlinearity, multiphoton transitions, and intensity-dependent coupling in preserving entanglement [26,27,28,29,30,31,32,33,34,35].

In addition to entanglement, quantum teleportation serves as a fundamental protocol in quantum information theory, enabling the transfer of unknown quantum states using previously shared entanglement and classical communication [36,37]. The success of teleportation protocols is closely related to the fidelity of the transmitted state, which in turn depends on the quality of the shared entangled resource and the dynamical parameters of the system [38]. Studying teleportation fidelity in systems affected by nonlinear interactions, such as Stark shifts and Kerr media, provides valuable information on optimizing performance on realistic experimental platforms [39].

The main objective of this work is to explore how entropic uncertainty and entanglement behave in a two-atom cavity QED system and to investigate the performance of quantum teleportation using the same physical setup. We use the lower bound of the entropic uncertainty relation and concurrence as tools to characterize entanglement and its temporal evolution. Furthermore, we study how the teleportation fidelity varies with the system parameters, including input state angles and nonlinear coupling strengths.

This paper is organized as follows. Section 2 describes the physical model and presents the solution of the system dynamics. Section 3 outlines the entropic uncertainty framework. In Section 4, we investigate the influence of the Stark shift and Kerr medium on the witness to entanglement. Section 5 presents an analysis of the average teleportation fidelity within the same model. Finally, Section 6 concludes the paper with a discussion of our key findings.

2 The model and its solution

We use two-level atoms (A and B) and a single-mode cavity assisted by a nonlinear Kerr-like medium in our physical model. The two atoms are noninteracting and resonantly coupled with the single-mode cavity field. $|e\rangle$ and $|g\rangle$ will be used to mark the excited and ground states of each atom, respectively. The Hamiltonian of the system can be written as ($=1$) [40,41,42,43]:

$$H_{int} = \sum_{j=A,B} [a^{\dagger}a(\beta_2\sigma_j^{+}\sigma_j^{-} + \beta_1\sigma_j^{-}\sigma_j^{+}) + g(a^{\dagger 2}\sigma_j^{-} + a^{2}\sigma_j^{+})] + \chi a^{\dagger 2}a^{2}, \quad (2)$$

The photon generation (annihilation) operator in cavity mode is $a^{\dagger}(a)$, and the Stark shift parameters are β_2 and β_1. g controls the strength of the two-photon coupling between the atoms and the cavity. Furthermore, χ is the dispersive component in a third-order Kerr-like medium. σ_j^{+} and σ_j^{-} describe the raising and lowering operations, respectively. In Eq.2, σ_j^{+} and σ_j^{-} denote raising and lowering operations and are given by: $\sigma_j^{+} = |e\rangle_{jj}\langle g|$ and $\sigma_j^{-} = |g\rangle_{jj}\langle e|$ for a j^{th} two-dimensional atom. If the two atoms are initially formed in a maximally entangled state, they can be expressed in the form of Bell's state, which is $|\Psi_{atom}(0)\rangle = \frac{1}{\sqrt{2}}(|eg\rangle + |ge\rangle)$, if only a single photon is involved. This indicates that the cavity field is first defined by a Fock state, $|1\rangle$. Finally, the whole initial state of the model can be expressed as follows:

$$|\Psi(0)\rangle = \frac{1}{\sqrt{2}}(|eg\rangle + |ge\rangle) \otimes |1\rangle. \quad (3)$$

The time-dependent wave function for the current physical mode of the Fock state cavity and coupled atom is derived using the Schrodinger approach as:

$$|\Psi(t)\rangle = \alpha_1|eg1\rangle + \alpha_2|ge1\rangle + \alpha_3|gg3\rangle, \quad (4)$$

with probability amplitudes.

$$\alpha_1 = \alpha_2 = \frac{1}{\sqrt{2}\eta}\exp\left[-\frac{1}{2}igt\kappa\right](\eta\cos\left[\frac{1}{2}gt\eta\right] + i(5\gamma_1 - \gamma_2 + 6\chi_1)\sin\left[\frac{1}{2}gt\eta\right]),$$
$$\alpha_3 = \frac{-4\sqrt{3}i}{\eta}\exp\left[-\frac{1}{2}igt\kappa\right]\sin\left[\frac{1}{2}gt\eta\right], \quad (5)$$

where $\eta = \sqrt{(5\gamma_1+6\chi_1)^2-\gamma_2+48}$, $\kappa = 6\chi_1+\gamma_2+7\gamma_1$ and $\gamma_1 = \frac{\beta_1}{g}$, $\chi_1 = \frac{\chi}{g}$ and $\gamma_2 = \frac{\beta_2}{g}$. Using the field variables and taking the trace of the state given by Eq.(4), we get the statistical ensemble state of the atom-atom system $\rho_{AB}(t)$. On a standard basis $|ee\rangle$, $|ge\rangle$, $|eg\rangle$ and $|gg\rangle$, the relative atom-atom density ensemble $\rho_{AB}(t)$ takes the form of:

$$\rho_{AB} = \begin{pmatrix} 0 & 0 & 0 & 0 \\ 0 & \hat{\rho}_{22} & \hat{\rho}_{23} & 0 \\ 0 & \hat{\rho}_{32} & \hat{\rho}_{33} & 0 \\ 0 & 0 & 0 & \hat{\rho}_{44} \end{pmatrix} \tag{6}$$

where

$$\hat{\rho}_{22} = |\alpha_1|^2, \hat{\rho}_{33} = |\alpha_2|^2, \hat{\rho}_{44} = |\alpha_3|^2, \\ \hat{\rho}_{23} = \alpha_1\alpha_2^*, \hat{\rho}_{32} = \hat{\rho}_{23}^*. \tag{7}$$

3 The entropic uncertainty relation when related to a non-local memory

According to Eq. (1), we order $M = \sigma_x$ and $N = \sigma_y$

$$S(\sigma_x|B) + S(\sigma_y|B) \geq S(A|B) + \log_2(\frac{1}{c}), \tag{8}$$

where, for the states $\hat{\rho}_{AB}$, $\hat{\rho}_{\sigma_x B}$ and $\hat{\rho}_{\sigma_y B}$, the corresponding von Neumann conditional entropies can be expressed as:

$$S(A|B) = -S(\hat{\rho}_B) + S(\hat{\rho}_{AB}), \tag{9}$$
$$S(\sigma_x|B) = -S(\hat{\rho}_B) + S(\hat{\rho}_{\sigma_x B}), \tag{10}$$
$$S(\sigma_y|B) = -S(\hat{\rho}_B) + S(\hat{\rho}_{\sigma_y B}). \tag{11}$$

In addition, $S(\hat{\rho})$ is the von Neumann entropy, which can be computed using:

$$S(\hat{\rho}) = -tr(\hat{\rho}\log_2\hat{\rho}) = \sum_j \eta_j \log_2 \eta_j, \tag{12}$$

Note that we express the corresponding eigenvalues η_j of the density matrix $\hat{\rho}$. The states $\hat{\rho}_{\sigma_x B}$ and $\hat{\rho}_{\sigma_y B}$ are the post-measurement states after σ_x and σ_y are performed on the atom A, that is, $\hat{\rho}_{\sigma_x B} = \sum_m (|\psi_m\rangle\langle\psi_m| \otimes I_B)\hat{\rho}_{AB}(|\psi_m\rangle\langle\psi_m| \otimes I_B)$ and $\hat{\rho}_{\sigma_y B} = \sum_n (|\varphi_n\rangle\langle\varphi_n| \otimes I_B)\hat{\rho}_{AB}(|\varphi_n\rangle\langle\varphi_n| \otimes I_B)$, in which $|\psi_m\rangle$ and $|\varphi_n\rangle$ are eigenvectors of σ_x and σ_y, respectively, $c \equiv \max_{m,n}|\langle\varphi_m|\psi_n\rangle|^2 = \frac{1}{2}$. However, if A and B are disentangled, then $S(A|B) \geq 0$ along with $S(A|B)\log_2(1/c) \geq 1$. Thus, the entanglement between A and B is entirely dependent on the lower bound of the entropic uncertainty relations. As a result, the right-hand side of the inequality can capture the entanglement (8). This means that the entanglement between A and B exists only if $S(A|B) + \log_2(1/c) < 1$.

4 Numerical results and discussion

For the estimation of the entanglement in the current study, we choose the Wootters concurrence defined as [44,45]:

$$C = \max\left(0, \sqrt{\mathscr{L}_4} - \sqrt{\mathscr{L}_3} - \sqrt{\mathscr{L}_2} - \sqrt{\mathscr{L}_1}\right), \tag{13}$$

where, $\mathscr{L}_i$ are the eigenvalues of the matrix $\widetilde{\hat{\rho}} = \hat{\rho}_{AB}(\sigma_y \otimes \sigma_y)\hat{\rho}_{AB}^*(\sigma_y \otimes \sigma_y)$ in decreasing order. Using Eq. (6), the concurrence can be put into the form:

$$C = 2\max[0, |\hat{\rho}_{23}|]. \tag{14}$$

In addition, we set MU to represent the minimum entropic uncertainty computed on the right-hand side of the inequality (8). The time intervals of robustness to the entanglement witnessed are indicated by (T_{EW}) under the condition $MU < 1$. The term (C_{EW}) is used to show the degree of entanglement of the witness under the given condition of $MU < 1$. From the density matrix in Eq. (6), we get

$$MU = 1 - (\hat{\rho}_{44}\log_2[\hat{\rho}_{44}] + \varepsilon_1\log_2[\varepsilon_1] + \varepsilon_2\log_2[\varepsilon_2] \\ - \hat{\rho}_{33}\log_2[\hat{\rho}_{33}] - (\hat{\rho}_{44}+\hat{\rho}_{22})\log[\hat{\rho}_{44}+\hat{\rho}_{22}]), \tag{15}$$

where,
$\varepsilon_\pm = \frac{1}{2}\left(\hat{\rho}_{33}+\hat{\rho}_{22} \pm \sqrt{(-\hat{\rho}_{33})^2 + 4|\hat{\rho}_{23}|^2 + \hat{\rho}_{22}}\right)$

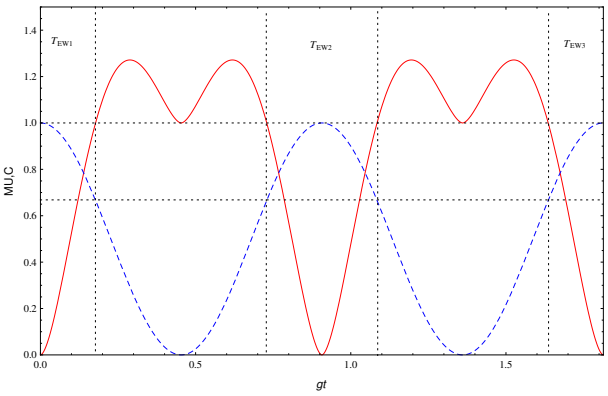

Figure 1: The dynamics of minimum uncertainty (MU solid-red) and concurrence (C dashed-blue) against gt, when $\gamma_1 = \gamma_2 = \chi_1 = 0$.

In Fig. 1, we present MU(solid-red) and C(dashed-blue) versus gt with the parameters set to $\gamma_1 = \gamma_2 = \chi_1 = 0$, when Stark shift effects and Kerr medium actions are absent. We observe that C decays from maximum to minimum values with a revival character as time t passes. The MU metric, on the other hand, has been revealed to have an inverse growth function, rising from a minimum to a maximum value (i.e., 1.27). The MU metric, like C, is showing indications of revival. This means that entanglement loss and entropy increase will be reversed under current conditions, and the state will become entangled and pure once more. This

contradicts the behavior of quantum systems coupled to local environments given in [46,47,48]. In actual quantum information processing, this could be advantageous for sharing information between the system and the environment, resulting in a prolonged preservation of the entanglement. Interestingly, in the interval of time $t \in \left[0, \frac{\pi}{\sqrt{3}}\right]$ there are three time zones and they are $T_{EW1} \in \left[0, \frac{1\pi}{10\sqrt{3}}\right]$, $T_{EW2} \in \left[\frac{4\pi}{10\sqrt{3}}, \frac{6\pi}{10\sqrt{3}}\right]$ and $T_{EW3} \in \left[\frac{9\pi}{10\sqrt{3}}, \frac{\pi}{\sqrt{3}}\right]$. The entanglement between A and B can be seen in these different time zones by $MU1$ being the same; there is always $C_{EW} =\in [0.686, 1]$. The current entropic uncertainty investigations and dynamical maps are completely different from those found in [49,50].

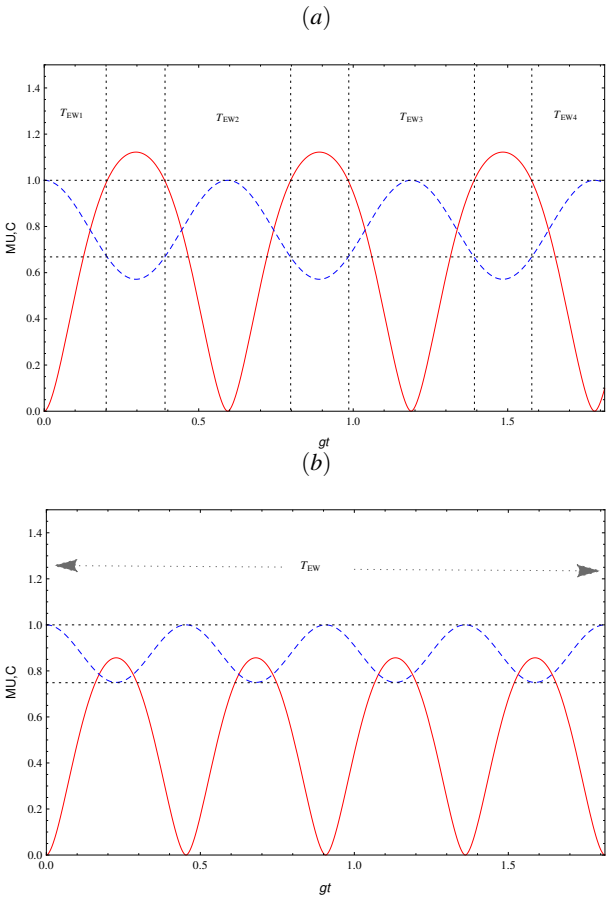

Figure 2: The dynamics of minimum uncertainty (MU solid-red) and concurrence (C dashed-blue) versus gt, with $\chi_1 = 0$, (a)$\gamma_1 = \gamma_2 = 4$ and (b) $\gamma_1 = \gamma_2 = 6$.

In Fig. 2, we describe the influences of the Stark shift on MU and C versus gt. In agreement with Fig.1, we find both the C and MU measures to grow oppositely at comparable times. Fig.2-(a) shows that when we set $\gamma_1 = \gamma_2 = 4$, C first decays from 1 to 0.57 and then oscillates between the maximum and minimum values. In addition, MU increases from zero to 1.123 and then shows revivals for the increasing choices of t. Comparing Fig.1 and Fig.2-a, it is easy to deduce that the corresponding dynamical maps are similar, but revival entanglement and entropic uncertainty are more dominant in the current case. Unlike Fig.1, we noticed that four different time zones using MU are $T_{EW1} \in \left[0, \frac{11\pi}{10\sqrt{3}}\right]$, $T_{EW2} \in \left[\frac{215\pi}{1000\sqrt{3}}, \frac{44\pi}{100\sqrt{3}}\right], T_{EW3} \in \left[\frac{544\pi}{1000\sqrt{3}}, \frac{77\pi}{100\sqrt{3}}\right]$. and $T_{EW4} \in \left[\frac{87\pi}{100\sqrt{3}}, \frac{\pi}{\sqrt{3}}\right]$, there is always $C_{EW} =\in [0.668, 1]$. The number of time zones detected by MU expands when the Stark shift increases, allowing the entanglement between A and B to be observed using the lower bound of the entropic uncertainty relation, while C_{EW} remains invariant. This entropic uncertainty behaviour is against that shown in [51,52]. By increasing the Stark shift as shown in Fig.2-b, MU can detect the entanglement between A and B at any time. These time zones and entanglement revivals without complete suppression are completely lacking in local external fields, as seen in [53,54]. For our system under consideration, the critical values of the Stark shift at which the entanglement between A and B may be noticed by MU are $\gamma_1 = \gamma_2 = 4.88$.

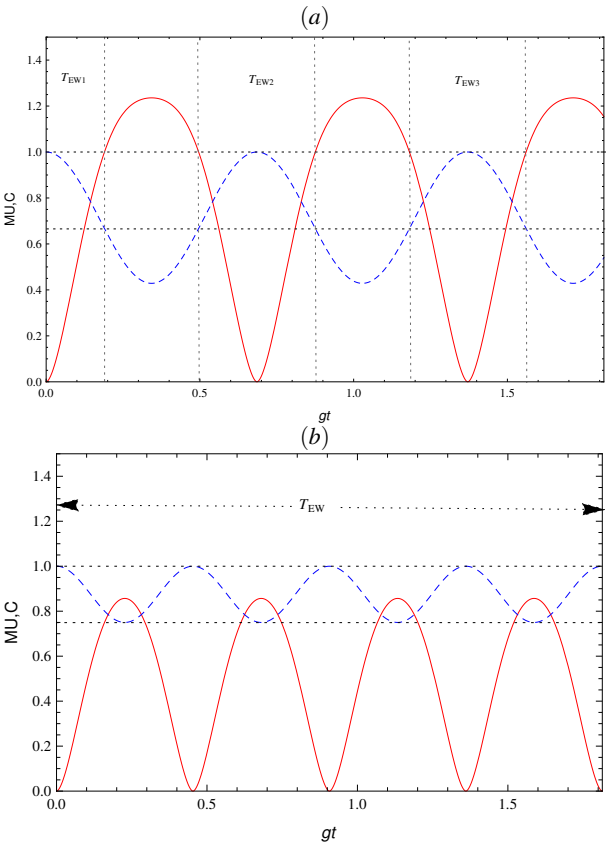

Figure 3: The dynamics of minimum uncertainty (MU solid-red) and concurrence (C dashed-blue) versus gt, with $\gamma_1 = \gamma_2 = 0$, (a) $\chi_1 = 1$, and (b) $\chi_1 = 2$.

In Fig.3, we analyze the impact of the Kerr medium on dynamical maps of MU and C. In Fig.3-a, we assign $\chi/g = 1$ and as time passes, we notice the C and MU measures growing or decreasing random functions of entanglement and entropic uncertainty. In addition, MU increases from a minimum to a maximum value of 1.123, but C decreases from a maximum to a minimum of 0.425. Both the C and MU measures show revivals of entanglement and entropic uncertainty and agree with Figs.1 and 2. There are three time zones; they are $T_{EW1} \in \left[0, \frac{11\pi}{100\sqrt{3}}\right]$, $T_{EW2} \in \left[\frac{276\pi}{1000\sqrt{3}}, \frac{482\pi}{1000\sqrt{3}}\right]$, and $T_{EW3} \in \left[\frac{653\pi}{1000\sqrt{3}}, \frac{86\pi}{100\sqrt{3}}\right]$, and the entanglement is observed when $MU < 1$ and in agreement with the previous Fig.1 and 2, $C_{EW} = \in [0.668, 1]$. However, in Fig. 3b, we increase the Kerr medium ($chi_1 = 2$) by increasing the time that oscillations occur in MU and C, and MU witnesses the entanglement during all times. The critical value of the Kerr medium in which we can obtain the entanglement encountered by MU is $\chi_1 = 1.63$, which deviates in fact from the studies given in [49,50,51,52]. By comparing Fig.2 and Fig. 3, it can be easily deduced that the dynamical maps of MU and C agree with each other. This means that the effects of the Stark shift, in addition to the Kerr medium, have the same impact on the time evolution of MU and C. However, for the different parameter values of both γ_1,γ_2 and χ_1. Our results show that we can obtain the time zones in which the entanglement witnessed by MU during all time increases by increasing the values of the Stark shift effect and the Kerr medium, which contradicts the intrinsic characters of local fields given in [46,47,48,53,54]. However, slight entanglement revivals were detected in different types of non-local systems and cavity interactions as given in [49,50]. Also, the critical value of the Kerr medium in which entanglement witnessed by MU during all time is less than the value of the Stark shift.

5 Quantum Teleportation

Quantum teleportation is one of the most well-known topics in quantum information theory, and its goal is to teleport an arbitrary quantum state [36]. The story of quantum teleportation is that Alice wishes to send an arbitrary quantum state to Bob. They agreed to use a quantum channel by a pair of entangled states and share it between themselves. Fidelity and average fidelity are two efficient measures that help us to determine the quality of teleportation [37]. We are interested in how close the output state is to the initial state. For an arbitrary two-qubit pure state, the input unknown state can be considered as

$$|\Psi_{in}\rangle = \cos(\frac{\theta}{2})|eg\rangle + e^{i\phi}\sin(\frac{\theta}{2})|ge\rangle. \quad (16)$$

with $0 \leq \theta \leq \pi$ and $0 \leq \phi \leq 2\pi$, where θ and ϕ are the amplitude and phase of the state, respectively.

Then, the output state is defined as

$$\rho_{out} = \sum_{i,j=0,x,y,z} \mathscr{P}_{i,j}(\sigma_i \otimes \sigma_j)\rho_{in}(\sigma_i \otimes \sigma_j), \quad (17)$$

where $\rho_{in} = |\Psi_{in}\rangle\langle\Psi_{in}|$, $\sigma_0 \equiv I$ is the identity matrix and $\sigma_{i,j}(i,j = x,y,z)$ are the Pauli matrices, $\mathscr{P}_{i,j} = Tr\left[\gamma^i\rho_{ch}\right]Tr\left[\gamma^j\rho_{ch}\right]$ in which $\sum_{i,j}\mathscr{P}_{i,j} = 1$, $\gamma^0 = |\Psi^-\rangle\langle\Psi^-|$, $\gamma^1 = |\Phi^-\rangle\langle\Phi^-|$, $\gamma^2 = |\Phi^+\rangle\langle\Phi^+|$ and $\gamma^3 = |\Psi^+\rangle\langle\Psi^+|$ with Bell states $|\Phi^\pm\rangle$ and $|\Psi^\pm\rangle$ [55,56]. Herein, we consider the density operator of the channel as $\rho_{ch} \equiv \rho_{AB}(t)$.
Now, we can obtain the output density matrix in the following form.

$$\rho_{\text{out}} = \begin{pmatrix} \rho_{11} & 0 & 0 & 0 \\ 0 & \rho_{22} & \rho_{23} & 0 \\ 0 & \rho_{23}^* & \rho_{33} & 0 \\ 0 & 0 & 0 & \rho_{44} \end{pmatrix}, \quad (18)$$

where

$$\rho_{11} = 0, \quad \rho_{22} = |\alpha_1|^2, \quad \rho_{33} = |\alpha_2|^2, \quad \rho_{44} = |\alpha_3|^2, \quad \rho_{23} = \alpha_1^*\alpha_2.$$

The quality of the teleported state is characterized by the fidelity measure $\mathscr{F}(\rho_{\text{in}}, \rho_{\text{out}})$, defined as [37].

$$\mathscr{F}(\rho_{in}, \rho_{out}) = \left[Tr\left(\sqrt{(\rho_{in})^{1/2}\rho_{out}(\rho_{in})^{1/2}}\right)\right]^2, \quad (19)$$

On the other hand, the average fidelity of teleportation $\mathscr{F}_A$ can be formulated as

$$\mathscr{F}_A := \frac{1}{4\pi}\int_0^{2\pi} d\phi \int_0^{\pi} \mathscr{F}(\rho_{in}, \rho_{out})\sin(\theta)d\theta. \quad (20)$$

Hence, one can obtain the analytical expression of the average fidelity of teleportation for our case as follows.

$$\mathscr{F}_A = \frac{1}{2}\Big(|\alpha_3|^2 - (|\alpha_3| - 2|\alpha_1|)\cos^2(\theta) + 4|\alpha_1|^2\big(1 + \sin^2(\theta)\big)\Big). \quad (21)$$

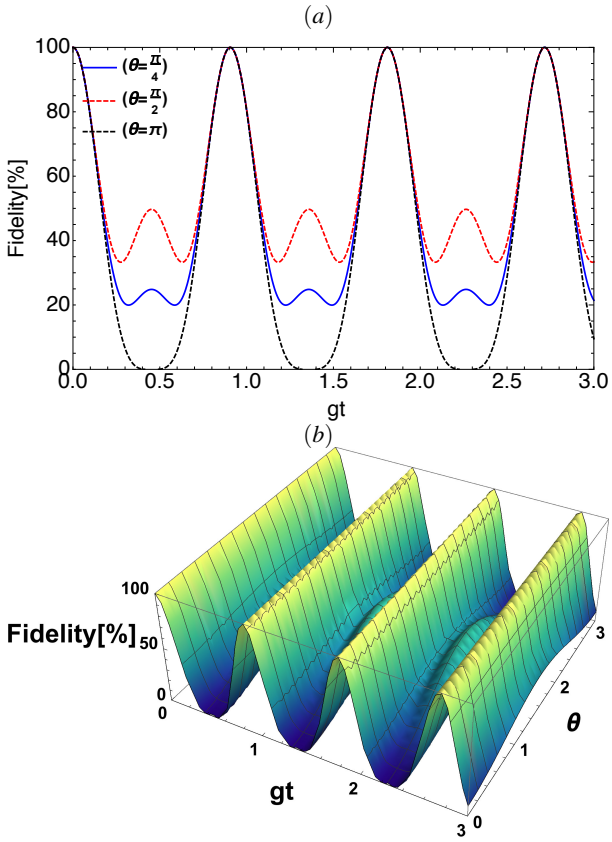

Figure 4: Time evolution of average fidelity as a function of gt when $\gamma_1 = 0.1$, $\gamma_2 = 0.5$ and $\chi_1 = 0.05$.

Fidelity is a crucial metric in quantum teleportation that quantifies the closeness between the teleported state and the original input state. A fidelity of 100% indicates perfect teleportation. Figures 4 and 5 systematically explore how fidelity evolves (gt) under different values of the input state angle θ, and the coupling parameter χ_1.

Figure 4 illustrates the time evolution of the average fidelity in a quantum teleportation protocol as a function of scaled time gt, with fixed parameters $\gamma_1 = 0.1$, $\gamma_2 = 0.5$, and $\chi_1 = 0.05$. Figure 4 (a) presents the dynamics of fidelity for three selected values of the input state angle θ, while figure 4 (b) shows a 3D surface plot of fidelity as a function of both gt and θ. Figure 4 (a) shows the evolution of fidelity for three different input state angles: $\theta = \frac{\pi}{4}$ (blue), $\frac{\pi}{2}$ (red) and π (black). A key observation is that all three curves reach identical peaks at specific time intervals, indicating periodic behavior in fidelity regardless of the initial state angle. However, the minimum fidelity values between peaks differ significantly. Specifically, the highest fidelity is achieved for $\theta = \pi$, suggesting that this input state is optimal for reliable teleportation. In contrast, $\theta = \frac{\pi}{4}$ produces the lowest fidelity in the valleys, emphasizing the importance of input state selection. Figure 4(b) illustrates the joint dependence of fidelity on both gt and θ. It confirms the periodic time dependence and highlights the sensitivity of fidelity to the input angle. High-fidelity regions appear periodically in both dimensions, indicating specific combinations of time and angle that optimize teleportation success. This analysis underlines the practical importance of parameter tuning in real-world quantum teleportation systems, particularly in setups influenced by nonlinear interactions such as Stark shifts and Kerr media [57,29,58,59,60].

Figure 5(a) shows the fidelity for different values of the non-linear coupling parameter $\chi_1 = 0$ (blue), 0.5 (red) and 1 (black), with $\gamma_1 = 0.1$, $\gamma_2 = 0.5$ and $\theta = \frac{\pi}{4}$ kept constant.

As χ_1 increases, the fidelity profiles change both in amplitude and frequency. In particular, for $\chi_1 = 1$, the fidelity achieves higher peaks compared to smaller values of χ_1. These variations suggest that the interaction strength introduces nontrivial modifications to the teleportation dynamics.

Figure 5(b) illustrates the fidelity as a function of gt and χ_1. The plot reveals periodic high-fidelity regions that depend on the strength and timing of the interaction. The nonlinear coupling parameter χ_1 significantly influences the fidelity of the teleportation, and the tuning χ_1 can be used as a control mechanism to optimize performance.

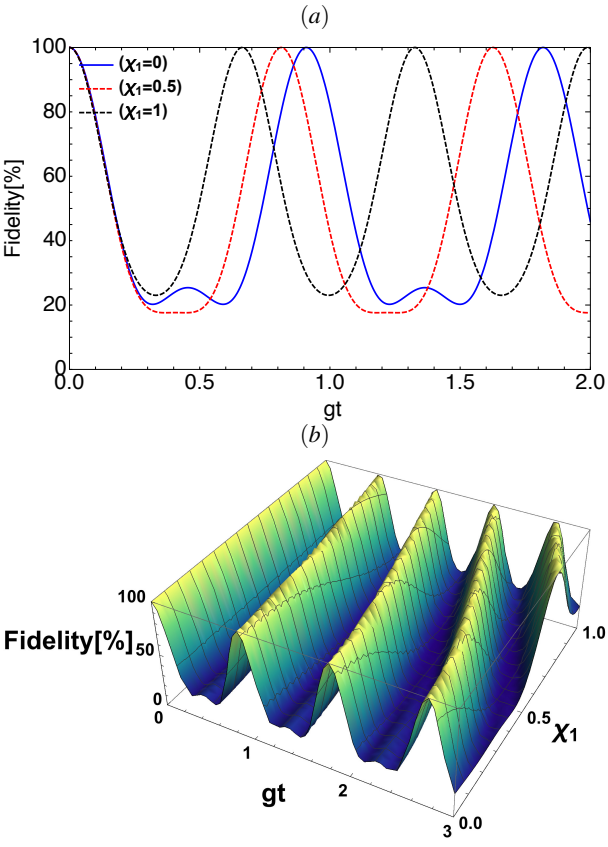

Figure 5: Time evolution of average fidelity as a function of gt when $\gamma_1 = 0.1$, $\gamma_2 = 0.5$ and $\theta = \frac{\pi}{4}$.

6 Conclusion

We have analyzed the dynamics of entanglement and entropic uncertainty in a system of two-level atoms interacting with a single-mode Fock state cavity field, both with and without the influence of the Kerr medium and Stark shift. Using concurrence and the lower bound of the quantum entropic uncertainty relation, we observed that entanglement undergoes sudden death and revival, rather than complete decay. The frequency of these entanglement revivals increases with higher values of the Kerr and Stark parameters, allowing for time regions where entanglement persists with minimal uncertainty.

Entropy, similar to entanglement, exhibits revivals and avoids permanent increase, reinforcing the system's resilience. These time-dependent behaviors provide a framework for engineering stable entangled states and minimizing information loss in quantum systems. The identified parameter regimes and time zones offer practical strategies for enhancing performance in quantum measurement, cryptography, and information processing. We examined average fidelity in a quantum teleportation protocol under nonlinear interactions. We found that increasing the angle of input state θ, particularly to π, and tuning the nonlinear coupling parameter χ_1, significantly improves fidelity. The fidelity shows a periodic dependence on the scaled time gt, highlighting the importance of precise parameter control and timing. Finally, our results provide valuable insights for designing robust quantum communication systems, where both entanglement dynamics and teleportation fidelity can be optimized through proper manipulation of physical parameters.

References

[1] W Heisenberg *Z. Physik* **43** (1927) 172–198
[2] I Bialynicki-Birula *Phys. Lett. A* **103** (1984) 253–254
[3] I Bialynicki-Birula J L and Madajczyk *Phys. Lett. A* **108** (1985) 384–386
[4] J A Vaccaro and R F Bonner *Phys. Lett. A* **198** (1995) 167–174
[5] M Berta, M Christandl, R Colbeck, J M Renes, and R Renner *Nat. Phys.* **6** (2010) 659–662
[6] A K Pati, M M Wilde, D A R Usha, A K Rajagopal and Sudha *Phys. Rev. A* **86** (2012) 042105
[7] N Zidan, *Entropy* **22** (2020) 837
[8] A.-H. Abdel-Aty, M. Omri, A.-B.A. Mohamed, and H. M. Rmili, *Alexandria Engineering Journal* **74** (2023) 21-28
[9] F. Panahyazdan, and A. Akhound, *Scientific Reports* **15** (2025) 12583
[10] Y.-Y. Fang, C. Zhang, and J.-M. Liu, *Physica A* **650** (2024) 129989
[11] C.-C. Liu, Z. W. Sun, X.-G. Fan, Z. Y. Ding, J. He, J. Wu, and L. Ye, *Scientific Reports* **15** (2025) 11386
[12] Liu, C., Liu, L., Cao, J., Abdel-Aty, M., *IEEE Transactions on Neural Networks and Learning Systems*, **34** (2021), 3992–4006
[13] Wang, Z., Cao, J., Lu, G., Abdel-Aty, M. (2020), *IEEE Transactions on Network Science and Engineering*, **7** (2019), 1814–1824
[14] Wang, Z., Cao, J., Cai, Z., Abdel-Aty, M. (2020), *Chaos*, **30** (2020), 013139
[15] Abdel-Aty, M., Moya-Cessa, H. , *Physics Letters A*, **369** (2007), pp. 372–376
[16] L Amico R Fazio A Osterloh and V Vedral *Rev. Mod. Phys.* **80** (2008) 517–576
[17] D Bouwmeester, J Pan, K Mattle M Eibl, H Weinfurter A Zeilinger *Nature* **390** (1997) 575–579
[18] N Zidan *Can. J. Phys.* **92** (2014) 406–410
[19] T Jennewein, C Simon G Weihs H Weinfurter and A Zeilinger *Phys. Rev. Lett.* **84** (2000) 4729
[20] M Tomamichel C C W Lim, N Gisin and R Renner *Nat. Commun.* **3** (2012) 634
[21] A Sorensen and K Molmer *Phys. Rev.* **A 62** (2000) 022311
[22] H Bakry A S A Mohamed and N Zidan *Int J Theor Phys* **57** (2018) 539–548
[23] L H Duan, A S Sorensen J I Cirac and P Zoller *Phys. Rev. Lett.* **85** (2000) 3991
[24] T Yu J H and Eberly *Phys. Rev. Lett.* **97** (2006) 140403
[25] M L Hu and F H Heng Fan *Phys. Rev.* **A 86** (2012) 032338
[26] H M Zou, M F Fang, B Y Yang, Y N Guo, W He and S Y Zhang *Phys. Scr.* **89** (2014) 115101
[27] M Abdel-Aty, M S Abdalla and A F Obada *J. Phys. B* **35** (2002) 807
[28] N Metwally, M Abdelaty and A F Obada *Optics Communications* **250** (2005) 148–156
[29] M Abdel-Aty *Physica A* **313** (2002) 471–487
[30] G M Nikolopoulos and P Lambropoulos *Journal of Modern Optics* **49** (2002) 61–71
[31] N Zidan, S Abdel-Khalek and M Abdel-Aty *Int. J. Quant. Inf.* **10** (2012) 1250007
[32] N Zidan *Physica A* **391** (2012) 401–409
[33] N Zidan *Int. J. Quant. Inf.* **8** (2010) 1121–1128
[34] M Abdel-Aty and N Zidan *Pramana – J. Phys. 61* (2003) 553–561
[35] M Akremi, S T Korashy, T M El-Shahat, R Nekhili, Inamuddin, M Rahimi-Gorji and I khan, *Journal of the Taiwan Institute of Chemical Engineers* **105** (2019) 171–181
[36] Bennett, C.H., Brassard, G., Crépeau, C., Jozsa, R., Peres, A. and Wootters, W.K., *Physical Review Letters*, **70**, (1993) 1895
[37] Nielsen, M. A., and Chuang, I. L. *Cambridge university press*, (2010).
[38] Popescu, S. *Physical Review Letters*, **74**, (1995) 2619
[39] Xia, Y., Song, J., Lu, P. M., and Song, H. S. *Journal of Applied Physics*, **109**, (2011)
[40] R R Puri and R K Bullough *J. Opt. Soc. Am. B* **5** (1988) 2021–2028
[41] T Nasreen and M S K Razmi *Phys. Rev. A* **46** (1992) 4161
[42] O Xi-Cheng, F Mao-Fa, K Guo-Dong, D Xiao-Juan and H Li-Yuan *Chin. Phys. B* **19** (2010) 030309
[43] H Yao-Hua and F Mao-Fa *Chin. Phys. B* **19** (2010) 070302
[44] S Hill and W K Wootters *Phys. Rev. Lett.* **78** (1997) 5022
[45] W K Wootters *Phys. Rev. Lett.* **80** (1998) 2245
[46] A U Rahman, M Noman, M Javed and A Ullah *Eur. Phys. J. Plus* **136** (2021) 846

[47] H Nha and H J Carmichael *Phys. Rev. Lett.* **93** (2004) 020401
[48] A U Rahman, M Noman, M Javed, M XM Luo and A Ullah *Quantum Inf Process* **20** (2021) 290
[49] S Haddadi, M R Pourkarimi, A Akhound and M Ghominejad *Laser Phys. Lett.* **16** (2019) 095202
[50] Z Huang *Quantum Inf. Process.* **17** (2018) 154
[51] X Xu and M F Fang *Chin. Phys. B* **29** (2020) 040306
[52] A L Zhou, D Wang, F Ming, W N Shi, J Yang and L Ye *Eur. Phys. J. Plus* **135** (2020) 489
[53] A U Rahman, M Javed, A Ullah and Z Ji *Quantum Inf Process* **20** (2021) 321
[54] A U Rahman, M Noman, M Javed, A Ullah and M X Luo *Laser Phys.* **31** (2021) 115202
[55] M Freitas, C Filgueiras, and M Rojas *Ann. der Phys.* **531**, (2019) 1900261
[56] S Ahadpour, and F Mirmasoudi *J. Super. and Novel Magn.* **33**, (2020) 3643–3649
[57] Abdalla, M.S., Abdel-Aty, M., Obada, A.-S.F., *Journal of Optics B* **4**(2002), 396–401
[58] Abdalla, M.S., Obada, A.-S.F., Abdel-Aty, M., *Annals of Physics*, **318** (2005), 266–285
[59] Abdel-Aty, M., Abdel-Khalek, S., Obada, A.-S.F., *Optical Review*, **7** (2000), 499–504
[60] Obada, A.-S.F., Abdel-Hafez, A.M., Abdelaty, M., *European Physical Journal D*, **3** (1998), 289–294